



SPE 90159

Assessment of Mud-Filtrate Invasion Effects on Borehole Acoustic Logs and Radial Profiling of Formation Elastic Parameters

Shihong Chi, SPE, Carlos Torres-Verdin, SPE, Jianghui Wu, SPE, Omer F. Alpak, SPE, The University of Texas at Austin

Copyright 2004, Society of Petroleum Engineers Inc.

This paper was prepared for presentation at the SPE Annual Technical Conference and Exhibition held in Houston, Texas, U.S.A., 26–29 September 2004.

This paper was selected for presentation by an SPE Program Committee following review of information contained in a proposal submitted by the author(s). Contents of the paper, as presented, have not been reviewed by the Society of Petroleum Engineers and are subject to correction by the author(s). The material, as presented, does not necessarily reflect any position of the Society of Petroleum Engineers, its officers, or members. Papers presented at SPE meetings are subject to publication review by Editorial Committees of the Society of Petroleum Engineers. Electronic reproduction, distribution, or storage of any part of this paper for commercial purposes without the written consent of the Society of Petroleum Engineers is prohibited. Permission to reproduce in print is restricted to a proposal of not more than 300 words; illustrations may not be copied. The proposal must contain conspicuous acknowledgment of where and by whom the paper was presented. Write Librarian, SPE, P.O. Box 833836, Richardson, TX 75083-3836, U.S.A., fax 01-972-952-9435.

Abstract

Despite continued improvements in acoustic logging technology, logs processed with industry standard methods often remain influenced by formation damage and mud-filtrate invasion. Proper quantitative understanding of the process of mud-filtrate invasion is necessary to identify and assess biases in the standard estimates of in-situ compressional- and shear-wave velocities. We describe a systematic approach to quantify the effects of mud-filtrate invasion on borehole acoustic logs and introduce a novel algorithm to estimate radial distributions of elastic parameters away from the borehole wall. Radial saturation distributions of mud filtrate and connate formation fluids are obtained by simulating the process of mud-filtrate invasion. Subsequently, radial profiles of the elastic properties are calculated using the Biot-Gassmann fluid substitution model. Array waveforms are simulated using the calculated radial profiles of formation elastic parameters as input. Estimated compressional- and shear-wave velocities for homogeneous, stepwise, and multilayered formation model are compared to quantify mud-filtrate invasion.

A nonlinear Gauss-Newton inversion algorithm is used to estimate radial profiles of formation elastic parameters in the presence of invaded zones using normalized spectral ratios of array waveform data. Inversion examples using synthetic and field data indicate that physically consistent profiles of formation elastic parameters can be reconstructed from array waveform data. In turn, radial profiles of formation elastic parameters can be used to construct more realistic near-wellbore petrophysical models for applications in reservoir simulation and production.

Introduction

During and after drilling, the near-wellbore formation is often altered by stress and stress release, mud-filtrate invasion,

chemical reactions, and many other factors. These alterations cause the physical properties in the near-wellbore region to be different from those of the uninvaded rock formation. Stress concentration around a wellbore may cause formation anisotropy and radial variation of velocities. The stress-induced anisotropy can be identified by dispersion analysis¹. Positive radial velocity gradients focus the elastic waves propagating away from the wellbore back toward the borehole wall. This phenomenon can be easily identified from high-amplitude acoustic arrivals. In well-consolidated hard rock formations, mechanical damage is less pronounced than in soft formations and is a much more localized phenomenon than mud-filtrate invasion effects. In this paper, we focus our attention to mud-filtrate invasion effects only.

It is well known that formation properties inferred from wireline logging measurements may not be the true properties of virgin formations. A realistic description of the invaded zone is important for the processing and interpretation of logs. Conventionally, in a damaged zone, the P-wave velocity of the formation near the wellbore is lower than the P-wave velocity of the virgin formation. In a flushed zone, the P-wave velocity is higher than that of the virgin formation. A common model used in the open literature assumes that a sharp interface exists between the altered zone and the undisturbed formation². The term “stepwise” is used to describe this type of mud-filtrate invasion model. Linear gradient models have been described for the syntheses of acoustic waveforms as well³. Actual radial profiles of elastic wave properties resulting from invasion can be quite complex and are dependent on the specific petrophysical properties of the rock as well as on the static and dynamic properties of the fluids involved. We describe a procedure for calculating the radial profiles of formation elastic properties with the Biot-Gassmann fluid substitution model starting from the numerically simulated fluid saturation profiles.

Theoretical and experimental studies⁴⁻¹⁰ have shown that rocks saturated with hydrocarbons and water can be differentiated with acoustic velocity measurements. Using time-lapse acoustic logging, bypassed zones can be identified and fluid movement in rock formations can be monitored in open- and cased-holes. It has been shown that a low frequency dipole tool senses 2-3 borehole diameters into the formation¹. If the invasion depth is approximately within 2-3 borehole diameters, the dipole tool can measure virgin formation properties. High frequency monopole tools penetrate one borehole diameter, thereby sensing only the damaged zone. If

the invasion depth is beyond the depth of investigation of a logging tool, the measured velocities will reflect those of the damaged zone and log corrections will be necessary to estimate virgin formation velocities.

Current industry practice of acoustic data processing makes use of the slowness-time coherence (STC) method to estimate in-situ velocities of rock formations. This type of processing yields values of P- and S-wave velocities, both of which are complex functions of formation and borehole properties, frequency, and number of time samples used in the window of the STC algorithm. When near-wellbore formation damage is significant, velocity logs obtained with the STC method may only reflect properties of the damaged zone even though modern acoustic tools are designed to sense past the damaged zone with the use of long source-receiver spacings and relatively low source frequencies. However, measured arrival times will be different in the presence of the damaged zone and will depend on the actual path that the elastic waves take from the source to the receivers. It becomes evident that using STC processing to estimate velocities neglects valuable information about near-wellbore formation properties.

In an effort to estimate near-wellbore formation properties, Hornby¹¹ developed a tomographic reconstruction technique that yielded formation compressional velocities near the wellbore from sonic travel times. The estimation was performed using a series of linear inversions followed by ray tracing. However, travel time tomography using ray tracing requires accurate picking of the refracted arrivals of each wave train and of the use of an accurate high-frequency ray-trace approximation. Furthermore, the method is limited to the reconstruction of the radial profile of compressional velocity in the near-wellbore region, even though estimation of formation shear wave velocity has long been one of the major objectives of full waveform acoustic logging.

Few studies on seismic full waveform inversion¹²⁻¹⁵ show that the use of amplitude data can improve the vertical resolution of one-dimensional radial distributions of velocity and density. Amplitude and phase behavior of full waveform data are sensitive to the petrophysical properties of formations supporting the propagation of elastic waves. Therefore, full-waveform analysis has a significant potential in acoustic logging to estimate petrophysical properties of damaged zones and virgin formations. The reconstruction of formation slowness away from the borehole wall can provide valuable calibration factors for measurements acquired with shallow reading devices, for example, bulk density logging. Corrections provided by full-waveform inversion may be of primary importance for the robust and accurate computation of synthetic seismograms. There is, however, one major difficulty to overcome in full waveform inversion. In all field applications, the effective source wavelet, the coupling among source, borehole, and formation, and the coupling between receivers and the formation depend on the in-situ borehole conditions. The practical difficulty in estimating the sonic source signature is probably the reason why very few attempts have been made to use the information borne by the full waveform of acoustic logging data.

Cheng¹⁶ described an indirect method for determining shear wave velocities from full waveform acoustic logs based on inversion. This method makes use of the spectral ratio of

the P-wave trains at two source-receiver separations, and simultaneously inverts for both formation shear-wave velocity and compressional wave attenuation. In this paper, Cheng's¹⁶ approach based on spectral ratio data is extended to full waveform arrays to overcome the practical difficulty of unknown source output spectrum. Lee and Kim¹⁷ estimated compressional velocity structures from synthetic seismic data by using a spectral ratio method. Frazer et al. and Frazer and Sun¹⁸⁻¹⁹ presented an inversion scheme for processing array full waveform data. Their approach does not require an exact source function although it is a necessary part of the inversion. Because of this, the chosen source function can affect the inversion results.

The inversion approach presented in this paper first transforms array waveforms into the frequency domain to construct a set of normalized array sonic data. The normalized wavefield is independent of the spectrum of the source, and hence the proposed inversion method allows one to make use of the full waveform content of sonic data without requiring knowledge of the source signature. Previous studies of full waveform borehole acoustic measurements assumed a homogeneous and isotropic formation and a model for borehole wave propagation without surface irregularities. The developments considered in this paper make the assumptions of a radially multilayered formation model and a cylindrical borehole.

Methodology

Numerical Simulation of Mud-Filtrate Invasion

Mud filtrate invasion is treated as a water or oil injection process into a gas or oil reservoir wherein two-phase immiscible fluid flow is assumed in the simulations. In order to study the effects of different types of mud filtration on gas or oil reservoirs, the following cases are selected: (a) water-base mud invades oil and gas reservoirs penetrated by open holes and (b) oil-base mud invades gas reservoirs penetrated by open holes. In each of these cases, it is assumed that a vertical well penetrates horizontally layered rock formations, and that the rock formation considered does not communicate hydraulically with its upper and lower shoulder beds. To study the sensitivity of mud-filtrate invasion to formation petrophysical properties, a low permeability (15 md) and low porosity (15 p.u.) reservoir and a high permeability (300 md) and high porosity (30 p.u.) reservoir are considered for cases (a) through (c).

Details of the numerical simulation of the process of mud-filtrate invasion in open holes can be found in Wu et al.²⁰ and George et al.²¹ In the simulations, both dynamic growth of mudcake and dynamic decrease of mudcake permeability are coupled to formation properties. This results in a dynamic monotonic decrease of flow rate into the formation. After a short initial spurt of mud-filtrate invasion, the invasion process reaches a steady state. Cycles of mudcake rub-off and buildup can also be taken into account.

A schematic of the process of mud filtrate invading a permeable rock formation is illustrated in Fig. 1. The invasion front moves deeper into the formation with time. Fig. 2 shows the time-evolution of water-base mud-filtrate saturation in the radial direction of a low-porosity, low-permeability, and oil-

bearing sandstone formation. The water-base mud filtrate reaches a radial distance of approximately 0.8 m after four days of invasion. Mud filtrate invasion is much shallower for the corresponding high porosity case. Fig. 3 shows that mud filtrate penetrates to a radial distance of 0.5 m after four days of invasion. For a gas-producing carbonate reservoir case (after George et al.²¹), mud filtrate reaches a radial distance of approximately 2 m after four days of invasion primarily due to the combined effects of a large overbalance pressure and low formation porosity (14 p.u.).

Oil-base mud invades the gas-bearing sandstone formation at a much slower rate. Fig. 4 shows that the time-evolution of oil-base mud-filtrate saturation in the radial direction of a low porosity (15 p.u.) and low permeability (30 md) formation. Oil-base mud filtrate reaches a radial distance of approximately 0.2 m after four days of invasion. Fig. 5 shows that mud filtrate primarily concentrates within a distance of 0.1 m away from the borehole wall.

Radial Profiles of Density and P- and S-Wave Velocities in an Invaded Zone

Once invasion profiles are obtained from numerical simulations, profiles of elastic formation properties can be calculated using the Biot-Gassmann fluid-substitution equations. Following the tutorial presented by Smith et al.²², a calculation is first performed of the basic formation and fluid properties. Subsequently, for each point in the saturation profile one can calculate: (a) fluid properties, (b) saturated bulk modulus of the rock, (c) bulk density of the rock, and (d) compressional- and shear- velocities.

When computing fluid and formation properties after invasion, a careful selection is necessary of homogeneous or patchy saturation models. Over geologic time, fluids in the pores of the rocks become homogeneously distributed. This is one of the important assumptions for the application of Biot-Gassmann's fluid-substitution model. However, mud-filtrate invasion in the near wellbore region changes the connate fluid distribution. From the numerical simulation results described in this paper, it is clear that the equilibrium of phases in the near-wellbore region is not established within a few days after the onset of the mud-filtrate invasion process. Wettability also causes segregated distribution of fluids. In the sonic logging frequency range, the time scale of wave propagation may be too short for the pressure to equilibrate. Therefore, it is more accurate to use a patchy saturation model to compute the corresponding bulk modulus²³.

Numerical Simulation of Time-Lapse Borehole Acoustic Measurements

Once the radial profiles of density and P- and S-wave velocities are obtained, they are discretized and approximated with a concentrically multi-layered rock model. The radial discretization is fine enough to ensure accurate representation of the continuous profiles. A corresponding stepwise-invaded zone model is also used for the numerical simulation. The waveforms simulated for the multilayered- and stepwise-models are compared against each other with the objective of assessing when the stepwise models will be adequate to represent the invaded zone.

In the synthesis of array waveforms, the assumption is made of a source-receiver configuration that replicates the Schlumberger's DSI tool. For the monopole mode, the central frequency of the source is 10 kHz. The minimum source-receiver distance is 9 ft with the receiver array consisting of 8 receivers spaced at 6 in intervals. Dipole modes make use of a 1.5 kHz source and a minimum source-receiver separation of 11.5 ft. In the Lower Dipole Mode, the 8 source-receiver offsets vary from 3.51 m (11.5ft) to 4.57 m (15ft) with a receiver spacing of 0.15 m (6 in). Sonic array waveforms are simulated for a homogeneous uninvaded formation as well as for the same formation after four days of mud-filtrate invasion.

Processing and Interpretation of Monopole and Dipole Logging Data

The sensitivity of acoustic measurements to different invasion models and radial saturation profiles can be assessed by comparing the synthetic waveforms for homogeneous, stepwise, and multi-layered radial formation models. Arrival times and amplitudes of P-, S-, and Stoneley-wave modes are the main waveform features used to assess the effect of mud-filtrate invasion on borehole acoustic logging measurements.

An industry standard slowness-time coherence (STC) method²⁴ is used to determine the velocities of P-, S-, and Stoneley-waves measured with array monopole logs. The STC method is well suited for non-dispersive waves. For the slightly dispersive Stoneley wave, the STC processing also provides accurate results. Interpolations in the time and slowness domains are performed to improve the accuracy of the computed velocities. The time-domain interpolation sharpens the peaks of coherence and hence the slowness-domain interpolation improves the accuracy of slowness at the respective contour peaks.

Radial depths of investigation for sonic tools depend on the formation type, shear and compressional slowness, the transmitter-to-receiver spacing, wavelength and wave mode considered, the source frequency, and the type of signal, among others. Frequency determines the wavelength that drives the depth of investigation of the measurement. Low frequency waves penetrate deeper into the formation and hence are sensitive to radial zones beyond invaded/damaged regions. As a rule of thumb, the depth of investigation is approximately one wavelength of the particular type of wave. Therefore, a dipole tool can investigate 3-4 times deeper than a monopole tool because the frequency of the dipole source is 3-4 times lower than that of the monopole source. Ideally, if the P- and S-wave velocities can be accurately determined, the depth of investigation can be determined by referring to the radial velocity profiles. However, the number of samples and frequency content in the correlation window influences the accuracy of the STC method. Measurements errors are approximately 1% for P-wave and 2% for S-wave velocities, respectively. Quite often, velocity variations due to mud-filtrate invasion remain close to such errors. For example, the maximum variation of V_p and V_s is about 2% and 4%, respectively, for a consolidated gas reservoir exhibiting 30% porosity. For a low porosity (less than 15%) reservoir, the velocity variation may not be distinguishable from processing errors.

The current industry standard for processing array dipole waveforms is the dispersive STC method. In this paper, the effect of invasion on dipole acoustic measurements is interpreted by directly comparing the characteristics of full waveforms.

When correlating seismic data with acoustic logs, it is often found that synthetic seismograms do not match the measured seismograms. As a result, corrections to the acoustic logs via Biot-Gassmann fluid substitution are common practice used in the seismic industry to rid sonic logs from mud-filtrate invasion effects. In this correction procedure, it is assumed that the measured velocities are those of the invaded zone saturated with mud filtrate. By displacing the saturation fluid in the invaded zone with the connate formation fluid and by applying the Biot-Gassmann fluid-substitution equation, new velocities are obtained and taken as virgin formation velocities. The validity of this practice is investigated through several case studies.

Full Waveform Inversion

The model of wave propagation in a borehole assumes an isotropic, radially multilayered formation, with no irregularities along the borehole wall. As with any inversion procedure, the accuracy and reliability of the results will depend on how accurately the forward model describes actual in-situ conditions. In practical field studies, irregularities on the borehole wall can be quantified using caliper measurements. Consequently, vertical intervals of formation can be identified that are consistent with the assumption of a smooth borehole wall. Along the length of the receiver spacing (6 in), the formation can be regarded as homogeneous in the axial direction.

In practice, the effect of borehole-receiver coupling can be assumed negligibly small in comparison to source coupling. The spectral ratio of the pressure responses at two receiver locations, z_1 and z_2 , from one common source can be written as

$$T_{12} = \frac{S(\mathbf{w}) \left[i \int_{-\infty}^{\infty} \frac{\hat{R}_{+}^{(1)} e^{ikp_f r_1}}{1 - \hat{R}_{+}^{(1)} e^{ikp_f r_1}} e^{ikz_2} dk + \frac{e^{ik_f z_2}}{z_2} \right]}{S(\mathbf{w}) \left[i \int_{-\infty}^{\infty} \frac{\hat{R}_{+}^{(1)} e^{ikp_f r_1}}{1 - \hat{R}_{+}^{(1)} e^{ikp_f r_1}} e^{ikz_1} dk + \frac{e^{ik_f z_1}}{z_1} \right]},$$

(1) where $S(\mathbf{w})$ is an effective source output spectrum. The source terms in equation (1) divide to 1, hence resulting in a final frequency representation independent of the source spectrum. This procedure indicates that, in principle, knowledge of the source spectrum is not necessary for full-waveform inversion when spectral ratios are used in inversion. In fact, the term T_{12} in equation (1) is the transfer function between the two receivers. For practical applications, the source functions are never fully known due to the variability of mechanical coupling due to vertical variation of formation properties. The source independent formulation described by equation (1) summarizes the conceptual basis for a robust and efficient algorithm that can be used as the forward computational model for full-waveform inversion. The transfer function T_{12} depends on both the formation and

borehole properties. Specifically, factors that affect the transfer function include (a) elastic parameters of the formation, (b) borehole radius R , (c) acoustic velocity V_f , (d) density ρ_f , and (e) quality factors for formation and borehole fluid. Toksöz et al.²⁵, Cheng et al.²⁶, and Cheng¹⁶ have assessed some of these factors using forward modeling techniques. Because the primary goal of this paper is to simultaneously invert radial profiles of density and P- and S-wave velocities, quality factors will not be subject to quantitative consideration. The normalized wavefield (or the normalized spectrum) of full-waveforms constitute the measurement data input to the full-waveform inversion algorithm. A cost function that enforces the least-squares difference between the simulated and measured normalized-wavefields is used for inversion. In order to quantify the robustness of the inversion algorithm, this paper also considers a sensitivity study to assess the influence of noise, normalization trace, and regularization parameter.

For the estimation of the radial distribution of elastic parameters, density and P- and S-wave velocities are assigned a constant value within each radial layer in the near-wellbore region. Let \mathbf{m} be the size- N vector of unknown parameters that fully describe the radial distribution of elastic parameters, and \mathbf{m}_R be a reference vector of the same size as \mathbf{m} that has been determined from some a-priori information. The estimation (inversion) of \mathbf{m} is undertaken from the measured data by minimizing a quadratic cost function, $C(\mathbf{m})$, defined as²⁷

$$2C(\mathbf{m}) = \left[\|\mathbf{W}_d \cdot [\mathbf{d}(\mathbf{m}) - \mathbf{d}^{obs}] \|^2 - \mathbf{c}^2 \right] + \mathbf{I} \|\mathbf{W}_m \cdot (\mathbf{m} - \mathbf{m}_R)\|^2, \quad (2)$$

where \mathbf{d}^{obs} is a size- M vector that contains the noisy measurements, and $\mathbf{W}_d \cdot \mathbf{W}_d^T$ is the inverse of the data covariance matrix. This data-weighting matrix describes the estimated variance for each particular measurement and the estimated correlation between measurements. The parameter \mathbf{c} denotes the prescribed value of enforced data misfit. A priori estimates of the noise in the measurements are employed to determine the magnitude of \mathbf{c} . In equation (2), $\mathbf{d}(\mathbf{m})$ is the measurement vector numerically simulated for specific values of \mathbf{m} , $\mathbf{W}_m \cdot \mathbf{W}_m^T$ is the inverse of the model covariance matrix, used to enforce both a quantitative degree of confidence in the reference model, \mathbf{m}_R , and a-priori information about \mathbf{m} , and \mathbf{I} is a Lagrange multiplier or regularization parameter.

The first additive term in the right-hand side of equation (2) drives the inversion toward fitting the measurements within the desired \mathbf{c}^2 value. The sole presence of such a term in the cost function $C(\mathbf{m})$, will yield multi-valued solutions of the inverse problem as a result of both noisy measurements as well as insufficient and imperfect data sampling. Enforcing an extremely small data misfit may result in estimated models with exceedingly large norms²⁷. The second additive term on the right-hand-side of equation (2) is used to reduce non-uniqueness and to stabilize the inversion in the presence of

noisy and sparse measurements. In this context, the Lagrange multiplier, \mathbf{I} , controls the relative weight of the two additive terms in the cost function. The developments considered in this paper make use of relatively large regularization parameter at the outset, which monotonically decreases according to the number of iterations and according to the observed reduction of the cost function from iteration to iteration.

Measurement and Model Vectors

In the cost function equation (2), the measurement vector \mathbf{d}^{obs} is constructed from the real and imaginary parts of the normalized spectra, $\text{Re}(S)$ and $\text{Im}(S)$, in the following organized fashion:

$$\mathbf{d}^{obs} = [\text{Re}(S_1), \text{Im}(S_1), \dots, \text{Re}(S_j), \text{Im}(S_j), \dots, \text{Re}(S_M), \text{Im}(S_M)]^T, \quad (3)$$

where $j = 1, 2, \dots, M$.

In equation (3), M is the number of actual frequency-domain measurements and the superscript T indicates transpose. The amplitude of the spectra can also be used as the measurement vector at the expense of losing phase information. The ordering procedure that assigns an index, j , to a given measurement is a function of frequency for the spectrum of each trace and receiver locations. Real and imaginary parts of one measurement are arranged next to each other. If the tool has NREC receivers, the normalized wavefield has NREC-1 traces because one trace is used to eliminate the source effect. If the number of frequencies used for each trace is NFREQ, the actual number of data points used for the inversion is $2M = 2 * \text{NFREQ} * (\text{NREC}-1)$.

Similarly, the model vector can be assembled as

$$\mathbf{m} = [V_{p1}, V_{p2}, \dots, V_{p1}, V_{s2}, \dots, V_{sN}, \mathbf{r}_1, \dots, \mathbf{r}_N]^T \quad (4)$$

for the simultaneous inversion of P- and S-wave velocities and density for each radial layer, where V_p , V_s , and \mathbf{r} denote P-wave velocity, S-wave velocity, and density in the radial layers numbered from 1 to N , respectively. By denoting the model parameters as \mathbf{m}_i , where $i = 1, 2, \dots, 3N$, equation (4) can be written as

$$\mathbf{m} = [\mathbf{m}_1, \mathbf{m}_2, \dots, \mathbf{m}_{3N}]^T. \quad (5)$$

Gauss-Newton Fixed-point Iteration Search

A Gauss-Newton fixed-point iteration search²⁸ is used to determine a stationary point, \mathbf{m} , where the cost function attains a minimum. This method considers only first-order variations of the cost function in the neighborhood of a local iteration point. The corresponding iterated formula can be written as

$$\mathbf{m}^{k+1} = [\mathbf{J}^T(\mathbf{m}^k) \cdot \mathbf{W}_d^T \cdot \mathbf{W}_d \cdot \mathbf{J}(\mathbf{m}^k) + \mathbf{I} \mathbf{W}_m^T \cdot \mathbf{W}_m]^{-1} \cdot \{ \mathbf{J}^T(\mathbf{m}^k) \cdot \mathbf{W}_d^T \cdot \mathbf{W}_d \cdot [\mathbf{d}(\mathbf{m}^k) - \mathbf{d}^{obs} + \mathbf{J}(\mathbf{m}^k) \cdot \mathbf{m}^k] + \mathbf{I} \mathbf{W}_m^T \cdot \mathbf{W}_m \cdot \mathbf{m}_R \} \quad (6)$$

subject to

$$l_i \leq m_i^{k+1} \leq u_i, \text{ where } i = 1, 2, \dots, N. \quad (7)$$

In the above two expressions, the superscript k is used as an iteration count, and $J(\mathbf{m})$ is the Jacobian matrix of $C(\mathbf{m})$. Upper and lower bounds enforced on \mathbf{m}^{k+1} are intended to

have the iterated solution yield only physically consistent results. The fixed-point iteration search for a minimum of $C(\mathbf{m})$ is concluded when the measured data have been fit within the prescribed tolerance, \mathbf{c}^2 .

Relative data misfits computed with the formula

$$\frac{\| \mathbf{W}_d \cdot [\mathbf{d}(\mathbf{m}^k) - \mathbf{d}^{obs}] \|^2}{\| \mathbf{W}_d \cdot \mathbf{d}^{obs} \|^2} \quad (8)$$

are used in this paper to enforce a convergence criterion.

Case Studies

Sandstone Oil Reservoir Invaded with a Water-Base Mud

In onshore conventional drilling activities, water-base mud is still widely used because of its efficiency to balance formation pressure without substantially increasing costs. Elastic properties of oil in rock formations are much closer to those of mud filtrate derived from a water-base mud. Compared to the case of mud filtrate invading a gas reservoir, it may be more difficult to distinguish mud-filtrate invasion effects on the measured velocities. Moreover, fluid-flow properties of oil and gas are also very different from each other. To study the sensitivity of the measured velocities to porosity and permeability, this section first considers a low porosity (15%) and low permeability (30 md) reservoir. Table 1 summarizes the petrophysical and fluid parameters used in the simulation of water-base mud-filtrate invasion. Subsequently, attention is focused to the case of a high porosity (30%) and high permeability (300 md) reservoir. Saturation profiles of mud filtrate and oil in formations are simulated for 4 days of invasion. The latter profiles are used to calculate radial profiles of elastic parameters using the Biot-Gassmann fluid-substitution model.

Fig. 2 shows the time evolution of mud-filtrate invasion for the case of water-base mud invading the oil-bearing sandstone reservoir of 15% porosity. Fig. 6 shows the radial profiles of the density and P- and S-wave velocities. P-wave velocities estimated from the array waveforms simulated for stepwise and multilayered models remain 1.1% lower than the true formation velocity. Moreover, these velocities do not exhibit the expected amount of increase in the invaded zone. It is therefore concluded that the P wave is sensitive to the radial region beyond the invaded zone. S-wave velocities remain 2% lower than that of the uninvaded formation. This indicates that S-wave propagation is sensitive to the invaded zone.

The radial profiles of density and P- and S-wave velocities are plotted in Fig. 7. STC results also show that the P wave is sensitive to the radial region beyond the invaded zone, whereas the S wave is sensitive to the invaded zone.

In summary, P waves are sensitive to virgin zones and S waves are sensitive to invaded zones when the length of mud-filtrate invasion is around 0.5-0.8 m in the two sandstone reservoirs considered in this section.

Sandstone Gas Reservoir Invaded with an Oil-Base Mud

In general, oil-base mud promotes shallower invasion than water-base mud and hence causes less formation damage. Since oil-base mud is also chemically less active compared to

water-base mud, it is more effective in inhibiting shale swelling. Because of this, oil-base mud is widely used to drill expensive offshore wells.

Two synthetic cases are selected to study mud-filtrate effects on the measured velocities of sandstone formations exhibiting low and high porosities and permeabilities.

For the gas-bearing sandstone reservoir of 15% porosity invaded with an oil-base mud, the radial profiles of the density and P- and S-wave velocities are shown in Fig. 8. Waveforms for the stepwise and multilayered models agree with each other. It is found that the P-wave amplitudes become much smaller in the presence of invasion, and that the S- and Stoneley-wave amplitudes increase considerably for monopole waveforms simulated for invaded formation models than for the virgin formation model. Dipole waveforms show that the S-wave amplitude also increases with the presence of invaded zones. The presence of oil-base mud filtrate reduces the P-wave arrival times, but does increase the S-wave arrival time. Arrival times for dipole waves remain unchanged.

P-wave velocities estimated from array waveforms simulated for stepwise and multilayered models are approximately 1.0% higher than the true formation P-wave velocity. S-wave velocities are approximately 0.2% lower than the true formation S-wave velocity. Therefore, P- and S-wave velocities are slightly influenced by mud-filtrate invasion, and remain primarily sensitive to the radial region beyond the invaded zone.

For the 30% porosity case, Fig. 9 shows the radial profiles of density and P- and S-wave velocities. It is observed from the monopole waveforms (Fig. 11) that the presence of invaded zones does not affect the P-wave arrival time, but it does delay the S-wave arrival time. On the other hand, P-wave amplitudes do not change appreciably, but S-wave amplitudes do increase. In the dipole waveforms, the change in S-wave arrival is negligible. Dipole waveforms for the stepwise model are significantly different from those simulated for the multilayered formation model.

By comparing the velocities for homogeneous, multilayered, and stepwise models, it is concluded that P waves penetrate past the invaded zone. S-wave velocities estimated for the stepwise and multilayered models are approximately 1% lower than that for the virgin formation. According to the Biot-Gassmann fluid substitution model, a rock formation saturated with 90% mud filtrate should exhibit a 4.3% S-wave velocity decrease compared to the S-wave velocity of the virgin formation. This indicates that the measured S-wave velocities remain influenced by mud filtrate in the near-wellbore region. Similar conclusions can be drawn from Fig. 11.

In all the cases studied in this section, both P and S waves are not sensitive to the invaded zones when the oil-base mud-filtrate invasion reaches a length of approximately 0.3 m in sandstone reservoirs.

Elastic Profiles of a Fast Rock Formation

This inversion case makes use of realistic elastic parameters for a fast formation model²⁹, which consists of six radial layers, including a fluid layer in the borehole. Table 3 describes the actual fluid and formation parameters and the radial discretization grid used for the inversion. Amplitude

spectra of the simulated waveforms indicate that the main energy is located within the frequency band 9-16 kHz. Data from the frequency band 11-14 kHz are used in the inversion to accelerate the convergence of the inversion algorithm.

Fig. 12 shows radial profiles and cross-plots of actual and inverted elastic parameters after 26 iterations of the inversion algorithm. The radial profiles of the inverted elastic parameters show a good agreement with the actual parameters. Global correlation coefficients are calculated between the inverted and the actual values of elastic parameters. All of the inverted elastic parameters exhibit high global correlation coefficients with the original model parameters (0.932, 1, and 1 for P- and S-wave velocities and density, respectively).

Elastic Profiles of a Slow Rock Formation

This example is an extension of the slow formation model in the simple borehole cases described by Cheng¹⁶ within the context of marine sediments. Table 4 describes the model, which consists of six radial layers, including one fluid layer in the borehole. The tool and source configurations are the same as those previously discussed for simple borehole cases. Given that the low frequency content of the full waveforms is more important in soft formations than in fast formations, data from the frequency band 2-5 kHz are used for inversion. Inversion results from this example not only estimate the virgin formation elastic parameter but also give a description of near-wellbore damage.

Inversions performed with no assumption of an increasing value of the elastic parameters away from the borehole wall converge to local minima without exception. Fig. 13 shows the profiles and the cross-plots of actual and inverted elastic parameters after 20 iterations for a slow formation under the assumption of monotonically increasing values of elastic parameters. The inversion also stops at a local minimum as can be observed from the evolution of the data misfit and cost functions shown in Figs. 13 (a) and 13(b), respectively. Global correlation coefficients for the inverted and the actual velocities are relatively high (0.83 and 0.83 for P- and S-wave velocities, respectively). However, for bulk density the correlation coefficient is -0.45. This indicates the relatively low sensitivity of the measurements in the frequency band (2-5 kHz) to radial variations of density. Overall, the inversion algorithm provides a way to estimate radial profiles of elastic parameters in soft rock formations. This is a valuable tool for detailed analysis of acoustic logging data in offshore wells.

Elastic Profiles from Field Data

This example assesses the feasibility and performance of the inversion algorithm when applied to field data. Full waveform acoustic data were acquired with the DSI tool in the depth from 13000 ft to 13050 ft within a well penetrating a tight-gas sandstone reservoir. Core data and log measurements indicate that the porosity of the fine-grained sandstone formation is below 9%. Gas saturation ranges from 80% to 95%. Fig. 14(a) is a display of the array waveform data acquired at the depth of 13030 ft. The bottom four traces show very similar characteristics in the number of wave modes and in the amplitudes of each wave mode. The top four traces, however, show a totally different character. Fig. 14(b) displays the amplitude spectra of the array waveform data. The main

energy of the waveforms is contained in the frequency band from 9 to 14 kHz. Input data to the inversion algorithm are chosen to be the normalized frequency data in the band of 11-14 kHz given that previous examples show that data from a narrower frequency data band improve the convergence of the algorithm. The STC processing method yields formation P- and S-wave slowness of 66.33 and 108.01 us/ft, which are used as the initial parameters for the inversion, respectively. Likewise, the density log reads a value of 2.504 gm/cc for bulk formation density. The mud density at this depth in the borehole is 14 ppg (1678 kg/m³), whereas the acoustic velocity of the mud is approximately 1186 m/s. Mud-filtrate invasion studies³⁰ indicate that mud filtrate reaches a radial distance of approximately 1.5 ft in the flow unit of interest after 24 hrs of drilling. Thus, a five-radial-layer model is used to describe the near-wellbore invasion zone. The inner radii of the radial formation layers are 0.07, 0.15, 0.30, 0.40, and 0.45 m, respectively, and the outmost layer is assumed to be unbounded in the radial direction. Within each radial zone, the formation elastic parameters are constant.

First, normalized frequency data from traces one to four in the band from 11 to 14 kHz are used as input data for the inversion. Data misfits decrease to 4% after 20 iterations. Fig. 14 (c) indicates that the formation P- and S-wave velocities increase and bulk density decreases in the radial direction. It is known that formation damage caused by drilling decreases the formation velocities and that mud-filtrate invasion in the near-wellbore region increases the bulk density. The inverted radial profiles indicate that a damaged zone exists in the near-wellbore region even though the borehole is in excellent condition. Such a result also agrees with the high-amplitude P-wave components that are observed from traces one through four of the array sonic waveforms. A radial profile of monotonically increasing P-wave velocity focuses the elastic waves propagating away from the wellbore back toward the borehole wall and increases the P-wave amplitude³¹⁻³². The radial profile of decreasing density can be interpreted as mud-filtrate displacing gas in the formation. This inversion exercise indicates that the algorithm can be used to estimate reliable radial profiles of formation elastic parameters in the near-wellbore region.

Conclusions

Direct comparison of time-lapse monopole waveforms shows that P wave arrives earlier, and that S- and Stoneley-waves arrive later for formation models with invaded zones than for homogeneous formation models in the cases of water-base mud invading oil-bearing sandstone reservoirs. P-wave amplitudes decrease by more than ten times because of the diverging effect of the monotonically decreasing profiles of density and P-wave velocity in the radial direction away from the borehole wall. On the other hand, S-wave amplitudes increase by a few percent due to the focusing effect of the monotonically increasing profiles of S-wave velocity in the radial direction. P waves are sensitive to virgin zones and S waves are affected by invaded zones when the length of invasion of mud-filtrate is around 0.5-0.8 m. For the cases of oil-base mud invading sandstone reservoirs, both P and S waves are insensitive to the presence of mud filtrate in the invaded zones.

The applicability of stepwise models for invaded zones depends on the shape of the fluid-saturation profiles in the invaded zones and on the length of mud-filtrate invasion. Time-lapse dipole waveforms show that the S-wave arrival is delayed by about the same amount with respect to monopole waveforms for the case of invaded formations.

Mud-filtrate invasion effects are not observed on P- and S-wave velocities estimated with industry standard STC processing for length of invasion around 2-3 borehole diameters. Therefore, log corrections are not necessary in these situations although discrepancies between seismic and acoustic velocities may still exist.

A novel full waveform inversion algorithm was developed that makes use of a normalized frequency spectrum. Normalized frequency spectrum for a source depends only on the borehole and formation models and on the position of the source, but does remain independent of the source spectrum. The validity of the algorithm was successfully assessed using radially multilayered 1-D synthetic models. An additional test of the inversion algorithm with field data acquired in a tight-gas reservoir also yielded petrophysically consistent results.

Inversions using the Gauss-Newton method yield radial profiles of formation density and P- and S-wave velocities for synthetic models. For the case of a multilayered slow formation, inversions using the low frequency array data converge to a local minimum. This indicates that the low frequency content of the full waveform data is sensitive to formation elastic parameters far from the borehole wall. For the case of a multilayered fast formation, data from the frequency band 11-14 kHz yielded radial profiles of formation elastic parameters that exhibited a very high correlation with the actual formation elastic parameters. This exercise showed that the high frequency component of the array sonic data may be preferable for estimating the radial distribution of elastic parameters in the near-wellbore region.

Acknowledgements

The work reported in this paper was funded by UT Austin's Research Consortium on Formation Evaluation, jointly sponsored by Baker Atlas, Halliburton, Schlumberger, Shell International E&P, and Anadarko Petroleum Corporation, ExxonMobil, ConocoPhillips, Total, and the Mexican Institute for Petroleum.

References

1. Plona, T., Sinha, B., Kane, M., Shenoy, R., Bose, S., Walsh, J., Endo, T., Ikegami, T., Skelton, O., 2002, Mechanical Damage Detection and Anisotropy Evaluation using Dipole Sonic Dispersion Analysis: Presented at the 43rd Ann. SPWLA Conf, Paper F, Osio, Japan.
2. Baker, L. J., 1984, The effect of the invaded zone on full wavetrain acoustic logging: *Geophysics*, 49, 796-809.
3. Stephen, R. A., Cardo-Casas, F., and Cheng, C. H., 1985, Finite-difference synthetic acoustic logs: *Geophysics*, 50, 1588-1609.
4. Geertsma, J., and Smit, D. C., 1961, Some aspects of elastic wave propagation in fluid-saturated porous solids: *Geophysics*, 26, 169-181.
5. Biot, M. A., 1956a, Theory of propagation of elastic waves in a fluid saturated porous solid I. Low-frequency range: *J. Acoust. Soc. Am*, 28, 168-178.

6. Biot, M. A., 1956b, Theory of propagation of elastic waves in a fluid saturated porous solid II. Higher frequency range: J. Acoust. Soc. Am., 28, 179-191.
7. Toksöz, M. N., Cheng, C. H., and Timur, A., 1976, Velocities of seismic waves in porous rocks: Geophysics, 41, 621-645.
8. Domenico, S. N., 1976, Effect of brine-gas mixture on velocity in an unconsolidated sand reservoir: Geophysics, 41, 882-894.
9. Dutta, N. C., and Ode, H., 1979a, Attenuation and dispersion of compressional waves in fluid-filled rocks with partial gas saturation White model: Part I-Biot theory: Geophysics, 44, 1777-1788.
10. Murphy, W. F. III, 1982a, Effects of microstructure and pore fluids on the acoustic properties of granular sedimentary materials: Ph.D. thesis, Stanford University.
11. Hornby, B. E., 1993, Tomographic reconstruction of near-borehole slowness using refracted borehole sonic arrivals: Geophysics, 58, 1726-1738.
12. Sen, M. K., and Stoffa, P. L., 1991, Nonlinear one-dimensional seismic waveform inversion using simulated annealing: Geophysics, 56, 1624-1638.
13. Zhou, C., Schuster, G. T., Hassanzadeh, S., and Harris, J. M., 1997, Elastic wave equation traveltimes and wavefield inversion of crosswell data: Geophysics, 62, 853-868.
14. Pratt, R. G., 1999a, Seismic waveform inversion in frequency domain, Part 1: Theory and verification in physical scale model: Geophysics, 64, 888-901.
15. Pratt, R. G., 1999b, Seismic waveform inversion in frequency domain, Part 2: Fault delineation in sediments using crosshole data: Geophysics, 64, 902-914.
16. Cheng, C. H., 1989, Full waveform Inversion of P waves for Vs and Qp: J. of Geophys. Res., 94, 15619-15625.
17. Lee, K. H., and Kim, H. J., 2003, Source-independent full waveform inversion of seismic data: Geophysics online, Published electronically on May 20, 2003.
18. Frazer, L. N., Sun, X., and Wilkens, R. H., 1997, Inversion of sonic waveforms with unknown source and receiver functions: Geophys. J. Int., 129, 579-586.
19. Frazer, L. N., and Sun, X., 1998, New objective functions for waveform inversion: Geophysics, 63, 213-222.
20. Wu, J., Torres-Verdín, C., Sepehrmoori, K., and Delshad, M., 2001, Numerical simulation of mud filtrate invasion in deviated wells: Paper SPE 71739, SPE Ann. Tech. Conf. and Exhib., New Orleans, Louisiana.
21. George, B. K., Torres-Verdín, C., Delshad, M., Sigal, R., Zouieueche, F., Anderson, B., 2003, A case study integrating the physics of mud-filtrate invasion with the physics of induction logging: assessment of in-situ hydrocarbon saturation in the presence of deep invasion and highly saline connate water: Presented at the 44th Ann. SPWLA Conf., paper K, Galveston, Texas.
22. Smith, T. M., Sondergeld, C. H., and Rai, C. S., 2003, Gassmann fluid substitutions: A tutorial: Geophysics, 68, 430-440.
23. Hill, R., 1963, Elastic properties of reinforced solids: Some theoretical principles: J. Mech. Phys. Solids, 11, 357-372.
24. Kimball, C.V., and Marzetta, T. L., 1984, Semblance processing of borehole acoustic array data: Geophysics, 49, 274-281.
25. Toksöz, M. N., Wilkens, R. H., and Cheng, C. H., 1985, Shear wave velocity and attenuation in ocean bottom sediments from acoustic log waveforms: Geophys. Res. Lett., 12, 37-40.
26. Cheng, C. H., Wilkens, and Meredith, J. A., 1986, Modeling of full waveform acoustic logs in soft marine sediments: 27th Trans. SPWLA Ann. Logging Symp., Paper LL, Houston, Texas.
27. Torres-Verdín, C., and Habashy, T. M., 1994, Rapid 2.5-dimensional forward modeling and inversion via a new nonlinear scattering approximation: Radio Science, 1051-1079.
28. Gill, P. E., Murray, W., and Wright, M. H., 1981, Practical optimization: Academic Press, London.
29. Schmitt, D. P., 1988, Shear wave logging in elastic formations: J. Acoust. Soc. of Am., 84, 2215-2229.
30. Salazar, J. M., Torres-Verdín, C., and Sigal, R., 2003, Facies and flow unit identification in a tight-gas hydrocarbon field: Presented at the 3rd annual Formation Evaluation Conference at the University of Texas at Austin, Austin, Texas.
31. Winkler K. W., 1997, Acoustic evidence of mechanical damage surrounding stressed boreholes: Geophysics, 62, 16-22.
32. Chen, X., Quan, Y., and Harris, J. M., 1996, Seismogram synthesis for radially layered media using the generalized reflection/transmission coefficients method: Theory and applications to acoustic logging: Geophysics, 61, 1150-1159.

Nomenclature

$S(\mathbf{w})$	=	Effective source output spectrum
T_{12}	=	Transfer function between the two receivers
R	=	Borehole radius
V_f	=	Acoustic velocity
\mathbf{m}	=	Size- N vector of unknown parameters
\mathbf{m}_R	=	Reference vector where \mathbf{d}^{obs} of size- M
$\mathbf{W}_d \cdot \mathbf{W}_d^T$	=	Inverse of the data covariance matrix between measurements
$\mathbf{d}(\mathbf{m})$	=	Measurement vector numerically simulated for specific values of \mathbf{m}
V_p	=	P-wave velocity
V_s	=	S-wave velocity
M	=	Number of frequency-domain measurements
T	=	Transpose
j	=	Index
NREC	=	Number of receivers
NFREQ	=	Number of frequencies used for each trace
Re	=	Real
Im	=	Imaginary

Greek Symbols

λ	=	Lagrange multiplier or regularization parameter
\mathbf{c}	=	Prescribed value of enforced data misfit
\mathbf{r}	=	Density

Table 1: Summary of geometrical, petrophysical, and fluid parameters used in the construction of sandstone reservoir models of water-base mud-filtrate invasion.

Variable	Units	Value
Mudcake Permeability	md	0.03
Mudcake porosity	fraction	0.30
Mud solid fraction	fraction	0.06
Mudcake maximum thickness	cm	1.00
Mudcake compressibility exponent	fraction	0.40
Mudcake exponent multiplier	fraction	0.10
Water viscosity (filtrate)	cp	1.00
Oil viscosity	cp	3.00
Rock compressibility	1/psi	0.0E-6
Water compressibility	1/psi	0.0E-6
Initial formation pressure	psi	5000.00
Mud hydrostatic pressure	psi	5500.00
Formation permeability	md	300.00
Formation porosity	fraction	0.25
Permeability anisotropy	fraction	1.00
Total invasion time	hours	48.00
Mudcake rub-off time	hours	36.00
Wellbore radius	cm	10.00
Mud filtrate salinity	ppm	43,900.00
Formation water salinity	ppm	102,500.00
Irreducible water saturation	fraction	0.1

Table 2: Summary of properties used in the fluid substitution model for sandstone reservoirs.

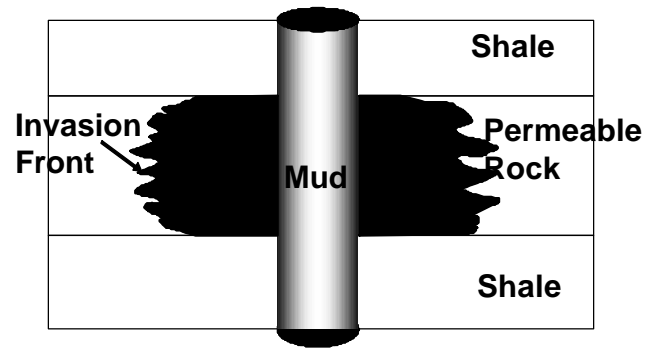
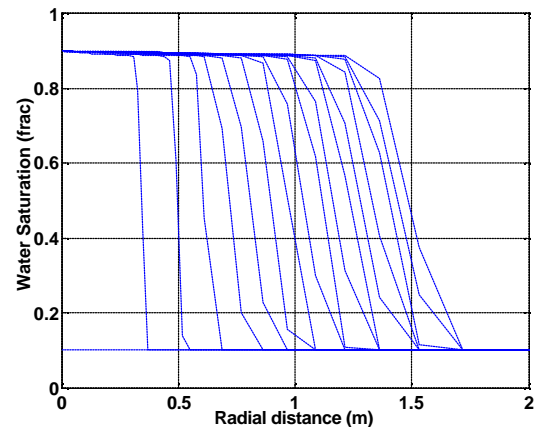
Bulk modulus of mineral matrix	GPa	3.0E10
Shear modulus of mineral matrix	GPa	1.0E10
Bulk density of mineral matrix	Kg/m3	2400
Bulk modulus of mud-filtrate	GPa	2.9E9
Density of mud-filtrate	Kg/m3	1055
Bulk modulus of oil	GPa	2.0E9
Density of oil	Kg/m3	800
Bulk modulus of gas	GPa	0.033
Density of gas	Kg/m3	100

Table 3: Description of the radial profiles of density and P- and S-wave velocities for the multilayered fast formation.

Layer	Inner radius (m)	ρ (g/cm ³)	V_p (m/s)	V_s (m/s)
1	0	1.0	1500	0
2	0.10	2.36	4390	2341
3	0.18	2.31	4512	2406
4	0.26	2.26	4634	2471
5	0.34	2.21	4756	2536
6	0.42	2.16	4878	2601

Table 4: Description of the radial profiles of density and P- and S-wave velocities for the multilayered slow formation.

Layer	Inner radius (m)	ρ (g/cm ³)	V_p (m/s)	V_s (m/s)
1	0	1.000	1500	0
2	0.10	2.000	2300	1000
3	0.18	2.025	2350	1060
4	0.26	2.050	2400	1120
5	0.34	2.075	2450	1180
6	0.42	2.100	2500	1240

**Fig. 1: Schematic of mud-filtrate invasion in rock formations penetrated by a mud-filled and overbalanced borehole.****Fig. 2: Time evolution of mud-filtrate invasion for the case of water-base mud invading a 15% porosity, oil-bearing rock formation. Plots of water saturation are shown for uniform time intervals of one day after the onset of mud-filtrate invasion. The first plot of water saturation corresponds to a time of one day after the onset of invasion.****Table 4: Description of the radial profiles of density and P- and S-**

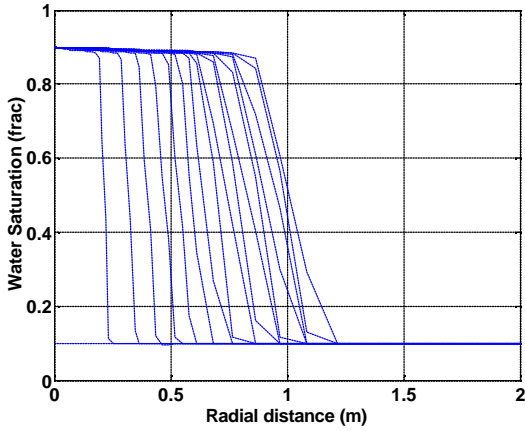


Fig. 3: Time evolution of mud-filtrate invasion for the case of water-base mud invading a 30% porosity, oil-bearing reservoir. Each line corresponds to one day of invasion.

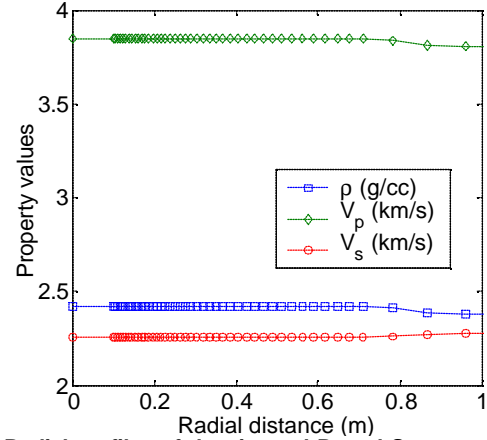


Fig. 6: Radial profiles of density and P- and S-wave velocities for the case of water-base mud invading a 15% porosity, oil-bearing reservoir after 4 days of invasion.

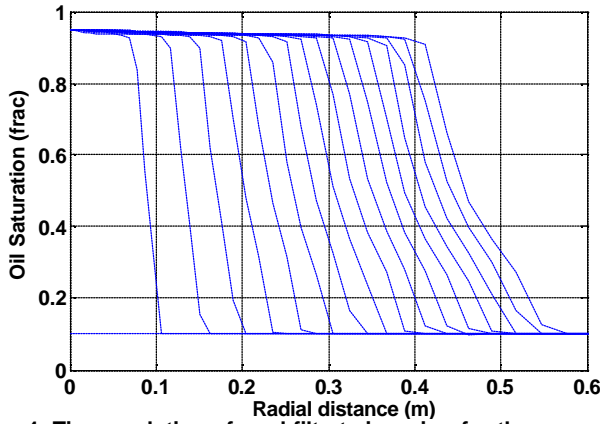


Fig. 4: Time evolution of mud-filtrate invasion for the case of oil-base mud invading a 15% porosity, gas-bearing reservoir. Each line corresponds to one day of invasion.

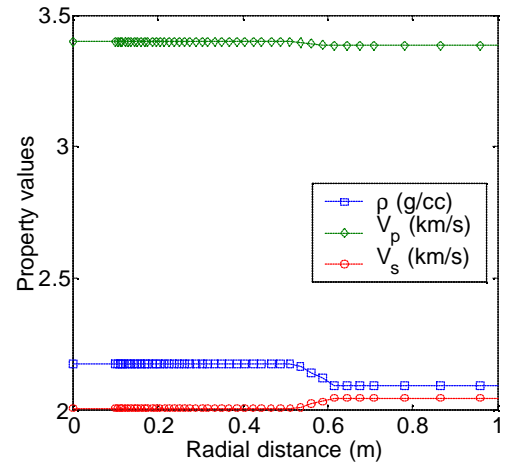


Fig. 7: Radial profiles of density and P- and S-wave velocities for the case of water-base mud invading a 30% porosity, oil-bearing rock formation after 4 days of invasion.

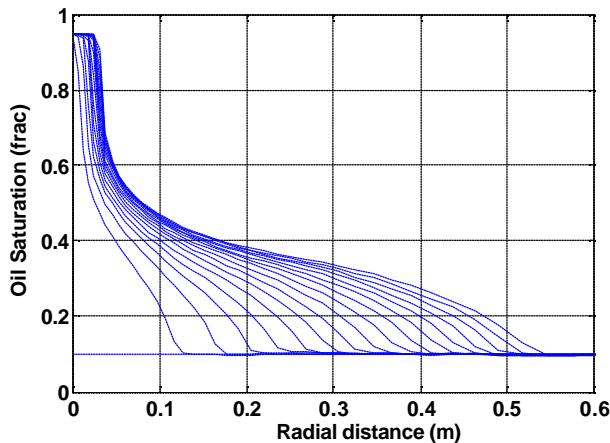


Fig. 5: Time evolution of mud-filtrate invasion for the case of oil-base mud invading a 30% porosity, gas-bearing reservoir. Each line corresponds to one day of invasion.

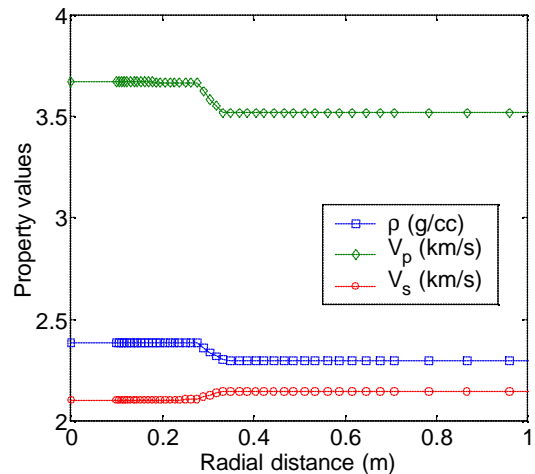


Fig. 8: Radial profiles of density and P- and S-wave velocities for the case of oil-base mud invading a 15% porosity, gas-bearing rock formation after 4 days of invasion.

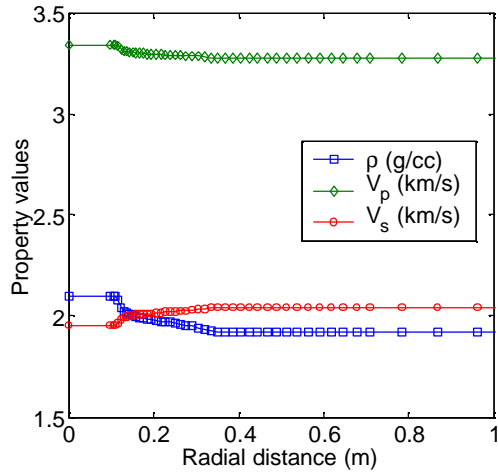


Fig. 9: Radial profiles of density and P- and S-wave velocities for the case of oil-base mud invading a 30% porosity, gas-bearing rock formation after 4 days of invasion.

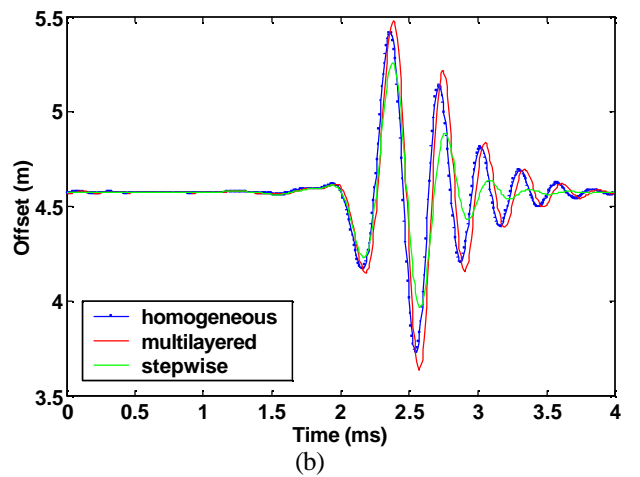
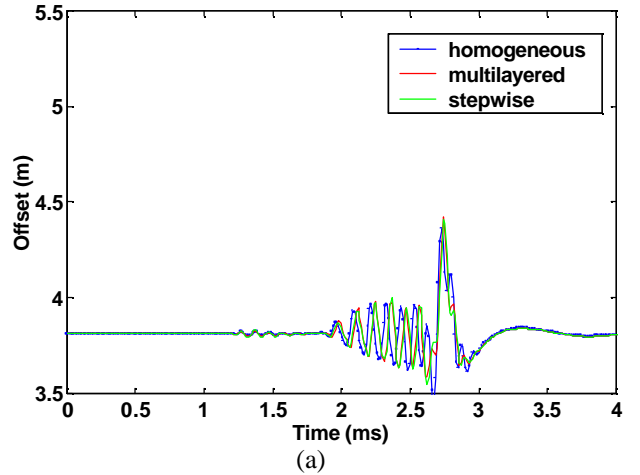


Fig. 11: Simulated (a) monopole and (b) dipole waveforms for the case of a homogeneous, stepwise, and multilayered formation model invaded with oil-base mud after 4 days of invasion in a gas reservoir with 30% porosity.

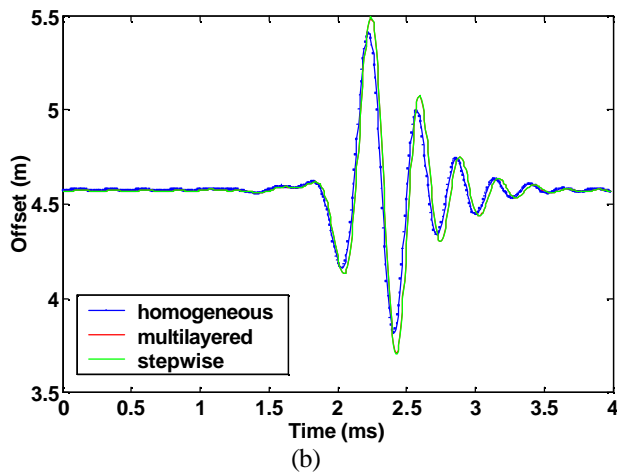
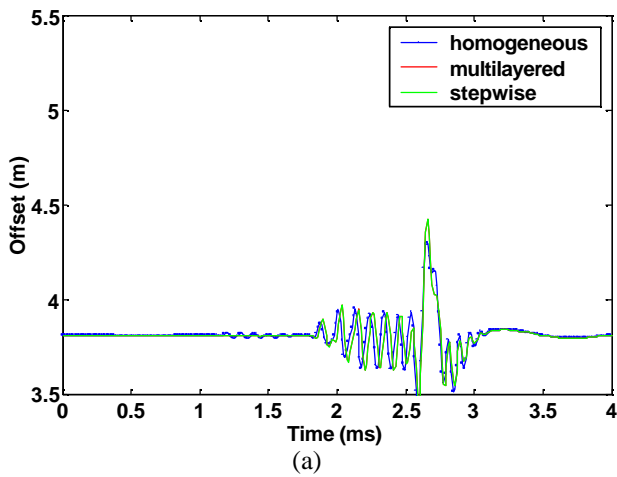
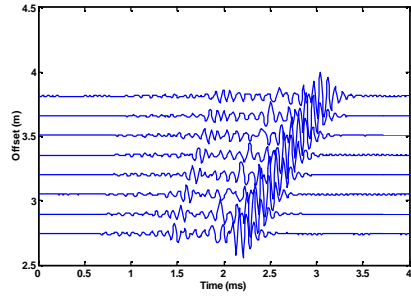
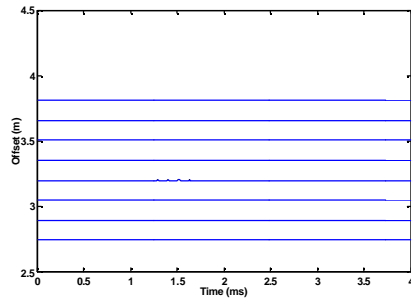


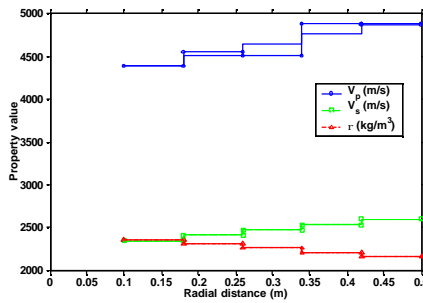
Fig. 10: Simulated (a) monopole and (b) dipole waveforms for the homogeneous, stepwise, and multilayered formation models shown in Fig. 6.



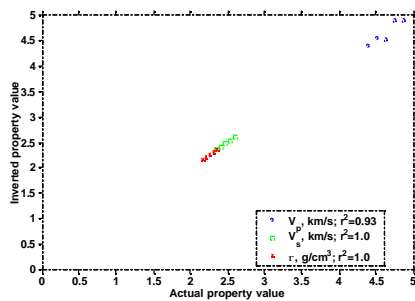
(a)



(b)

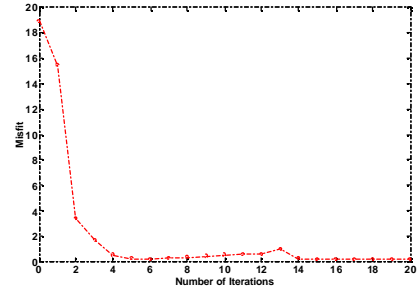


(c)

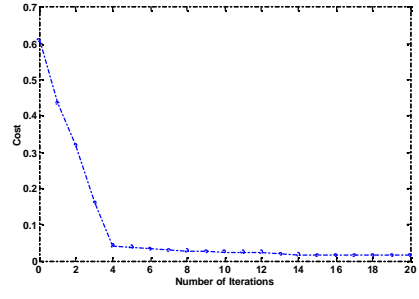


(d)

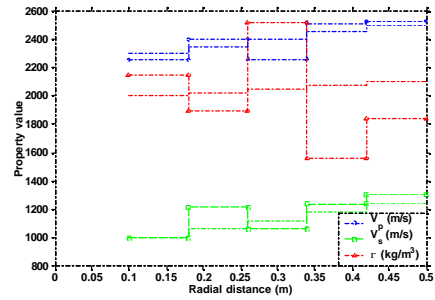
Fig. 12: Simultaneous inversion of radial profiles of elastic parameters for a six-layer fast formation using noise-free normalized spectra of array waveform data. Panel (a) shows the array waveform in the time domain and panel (b) shows the data residuals yielded by the inversion. In panel (c), the inverted radial distributions of elastic parameters are identified with solid lines and open circles, and in panel (b) r^2 is the correlation coefficient between the inverted and actual elastic parameters.



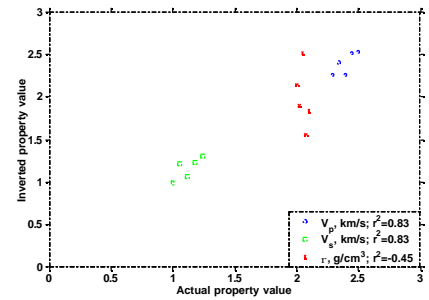
(a)



(b)



(c)



(d)

Fig. 13: Radial profiles and cross-plots of the actual and inverted elastic parameters for a six-layer slow formation. The evolution of the data misfit and cost functions with iteration number is shown in panels (a) and (b), respectively. In plot (c), the inverted radial distributions of elastic parameters are identified with open circles, and in plot (d) r^2 is the correlation coefficient.

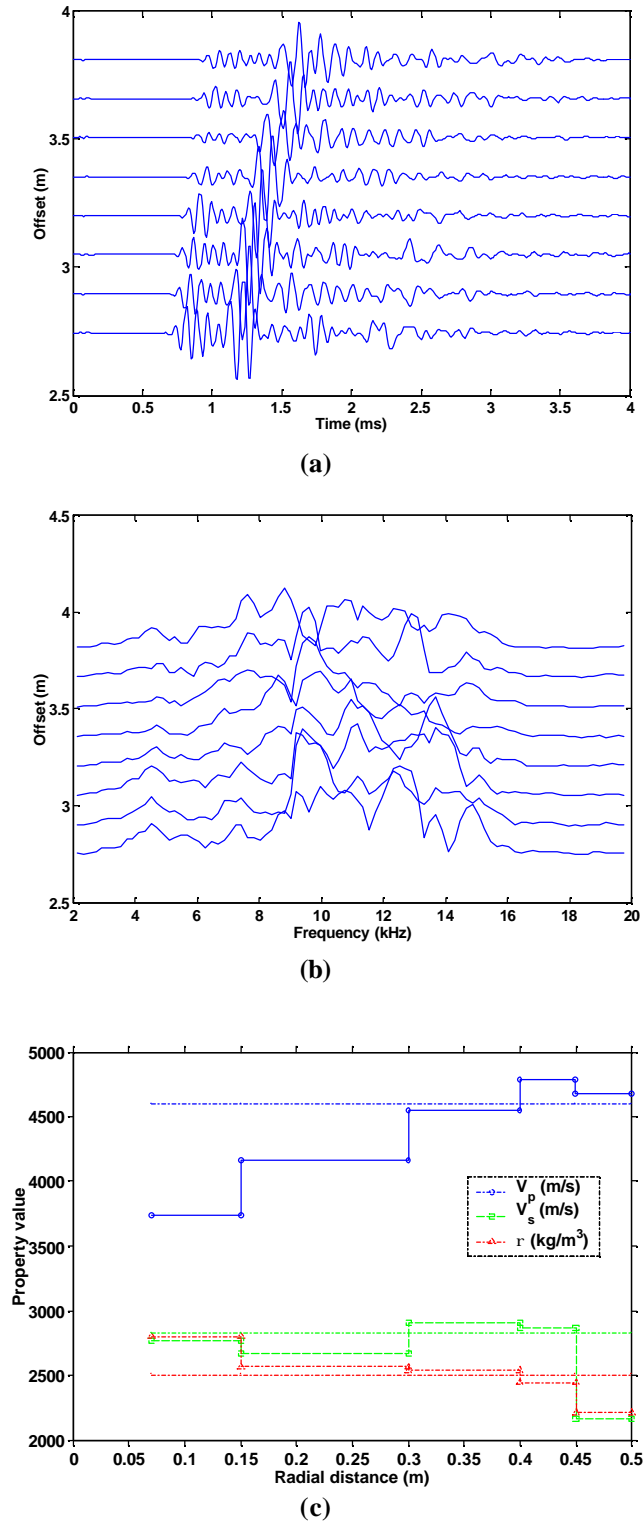


Fig. 14: Simultaneous inversion of radial profiles of elastic parameters using array waveform data acquired in the Anderson well No. 2 and penetrating a tight-gas reservoir. Panel (a) shows the array waveforms in the time domain and panel (b) shows the amplitude spectra. Panel (c) shows the homogeneous formation model used to initialize the inversion and the inverted radial profiles of formation elastic parameters.